Original Article

Construction and verification of an innovative immune-related and hallmark gene sets prognostic model for bladder cancer

Xiaoliang Zhou[1,2#], Yuejiao Liu[3#], Zhihong Lv[1,2#], Chong Shen[1,2], Shaobo Yang[1,2], Zhe Zhang[1,2], Ming Tan[4], Hailong Hu[1,2]

[1]Department of Urology, The Second Hospital of Tianjin Medical University, Tianjin, China; [2]Tianjin Key Laboratory of Urology, Tianjin Institute of Urology, Tianjin, China; [3]Department of Pharmacy, Zhu Xianyi Memorial Hospital of Tianjin Medical University, Tianjin, China; [4]Department of Urology, Tianjin Wuqing District Second People's Hospital, Tianjin, China

Contributions: (I) Conception and design: H Hu, M Tan; (II) Administrative support: H Hu, M Tan, C Shen; (III) Provision of study materials or patients: X Zhou, Y Liu, C Shen; (IV) Collection and assembly of data: X Zhou, C Shen, Z Zhang; (V) Data analysis and interpretation: C Shen, S Yang, Z Zhang; (VI) Manuscript writing: All authors; (VII) Final approval of manuscript: All authors.

[#]These authors contributed equally to this work.

Correspondence to: Hailong Hu, MD, PhD. Department of Urology, The Second Hospital of Tianjin Medical University, 23 Pingjiang Road, Jianshan Street, Hexi District, Tianjin 300211, China; Tianjin Key Laboratory of Urology, Tianjin Institute of Urology, Tianjin, China. Email: huhailong@tmu.edu.cn; Ming Tan, BS. Department of Urology, Tianjin Wuqing District Second People's Hospital, 961 Guangxian Road, Xiazhuzhuang Street, Wuqing Distric, Tianjin 301700, China. Email: tanming977@sina.com.

Background: Bladder cancer (BC) is a life-threatening malignancy with high mortality rates. Current prognostic models are insufficient in accurately predicting clinical outcomes, impeding personalized treatment strategies. This study aimed to identify BC subtypes and prognostic gene sets by analyzing changes in immune and hallmark gene sets activity in tumor and adjacent non-tumor tissues to enhance patient outcomes.

Methods: Utilizing data from The Cancer Genome Atlas (TCGA) and Gene Expression Omnibus (GEO), gene set variation analysis (GSVA) was applied to C7 immune-related and hallmark gene sets from the Molecular Signatures Database (MSigDB). The CancerSubtype R package was utilized for clustering these gene sets into three categories, from which 109 candidate sets were identified using Venn diagrams. A refined subset of seven gene sets was selected through least absolute shrinkage and selection operator (LASSO) regression for the construction of a risk model. Model validity was confirmed with receiver operating characteristic (ROC) and calibration curves, and a nomogram was constructed to integrate risk scores with clinical parameters. Finally, genes from the gene sets of the model were acquired and analyzed for Gene Ontology (GO) and Kyoto Encyclopedia of Genes and Genomes (KEGG) pathway enrichment and protein-protein interactions (PPI) via plugin Molecular Complex Detection (MCODE) and Search Tool for the Retrieval of Interacting Genes/Proteins (STRING) in Cytoscape in both tumor and non-tumor tissues.

Results: Three BC subtypes were characterized by immunologic and hallmark gene sets, with subtype 1 patients showing worse survival. The prognostic model, based on seven gene sets, effectively stratified risk, with high-risk patients having significantly shorter survival. GO, KEGG, and PPI analyses indicated distinct influences of non-tumor and tumor tissues on the prognosis of BC patients.

Conclusions: We constructed and validated a novel prognostic model for risk stratification in BC based on immunologic and hallmark genes sets, which presents a novel perspective on rational treatment approaches and accurate prognostic evaluations for BC by considering both tumor and adjacent non-tumor tissues. This highlights the importance of focusing on alterations in both tumor and adjacent non-tumor tissues, rather than solely on the tumor itself.

Keywords: Bladder cancer (BC); immunologic gene sets; hallmark gene sets; prognostic model; bioinformatics analysis

Submitted Feb 29, 2024. Accepted for publication Aug 01, 2024. Published online Sep 27, 2024.
doi: 10.21037/tcr-24-327
View this article at: https://dx.doi.org/10.21037/tcr-24-327

Introduction

Bladder cancer (BC) is a significant health issue, with muscle-invasive bladder cancer (MIBC) accounting for about 25% of cases and commonly leading to poor outcomes (1,2). The standard treatment has been radical cystectomy with cisplatin-based chemotherapy. However, the introduction of immune checkpoint blockade (ICB) therapies has yielded promising results for MIBC patients (3-6). Despite these advancements, the heterogeneity of BC, particularly in its response to immunotherapy, underscores the necessity for accurate prognostic models to enhance treatment strategies (7).

The tumor microenvironment (TME) plays a pivotal role in antitumor immunity, with natural killer (NK) cells being significantly influenced by cytokines such as interleukin-2 (IL-2). IL-2-expanded NK cells within The Cancer Genome Atlas bladder cancer (TCGA-BC) dataset have demonstrated prognostic value (8,9). This highlights the importance of understanding the immune landscape within BC for prognostication and treatment planning. To date, subtypes based on the activity changes of gene sets in BC have not been determined.

To address the challenge of prognostication, in this study, we conducted single sample gene set variation analysis (GSVA) with the GSVA R package to construct a prognostic prediction model based on immuneSigDB gene subsets of C7 and hallmark gene sets from the Molecular Signatures Database (MSigDB). Afterward, we identified three distinct BC subtypes characterized by the activity changes of immunologic gene sets and hallmark in BC and constructed a prognostic model using TCGA-BC dataset. The validity of this model was subsequently confirmed in Gene Expression Omnibus (GEO) cohorts. This research offers a unique approach to prognostic modeling in BC, shifting the focus from individual gene alterations to broader changes in gene sets activity within the BC population. This innovative model aims to reflect the complexity of the tumor immune microenvironment and aid clinical decision-making, thereby improving individualized treatment planning and advancing precision medicine in BC.

Moreover, this investigation sought to elucidate the functions of the genes, the signaling pathways, and the immune-related genes associated with the gene sets used for model construction. Our findings indicate that BC is highly correlated with the extracellular matrix, PIK3-Akt signaling pathway, and *EGFR* and *ITGA2* genes, offering deeper insights into the underlying mechanisms of BC progression and response to therapy. We present this article in accordance with the TRIPOD reporting checklist (available at https://tcr.amegroups.com/article/view/10.21037/tcr-24-327/rc).

Highlight box

Key findings

- The study identifies three distinct subtypes of bladder cancer (BC) characterized by differential immune-related and hallmark gene sets activities.
- A prognostic model based on seven gene sets was developed, which outperforms traditional staging systems in predicting patient survival.
- The analysis reveals that non-tumor tissues adjacent to bladder tumors also carry prognostic information, challenging the conventional focus on tumor tissues alone.

What is known and what is new?

- BC subtypes have been previously described based on histological and molecular features, but their prognostic implications are not fully understood.
- This manuscript introduces a novel approach to subtype classification using gene set activity analysis, providing deeper insights into the biological underpinnings of BC and their prognostic value.

What is the implication, and what should change now?

- The findings suggest that incorporating gene set-based subtyping into clinical practice could lead to more accurate prognostication and tailored treatment plans. Clinicians should consider integrating the new prognostic model into their assessment of BC patients, and research should further explore the role of non-tumor tissues in cancer progression and treatment response.

Methods

Study design

The workflow of this study is depicted in *Figure 1*.

Database

In this study, 425 BC samples, including 406 cancer samples

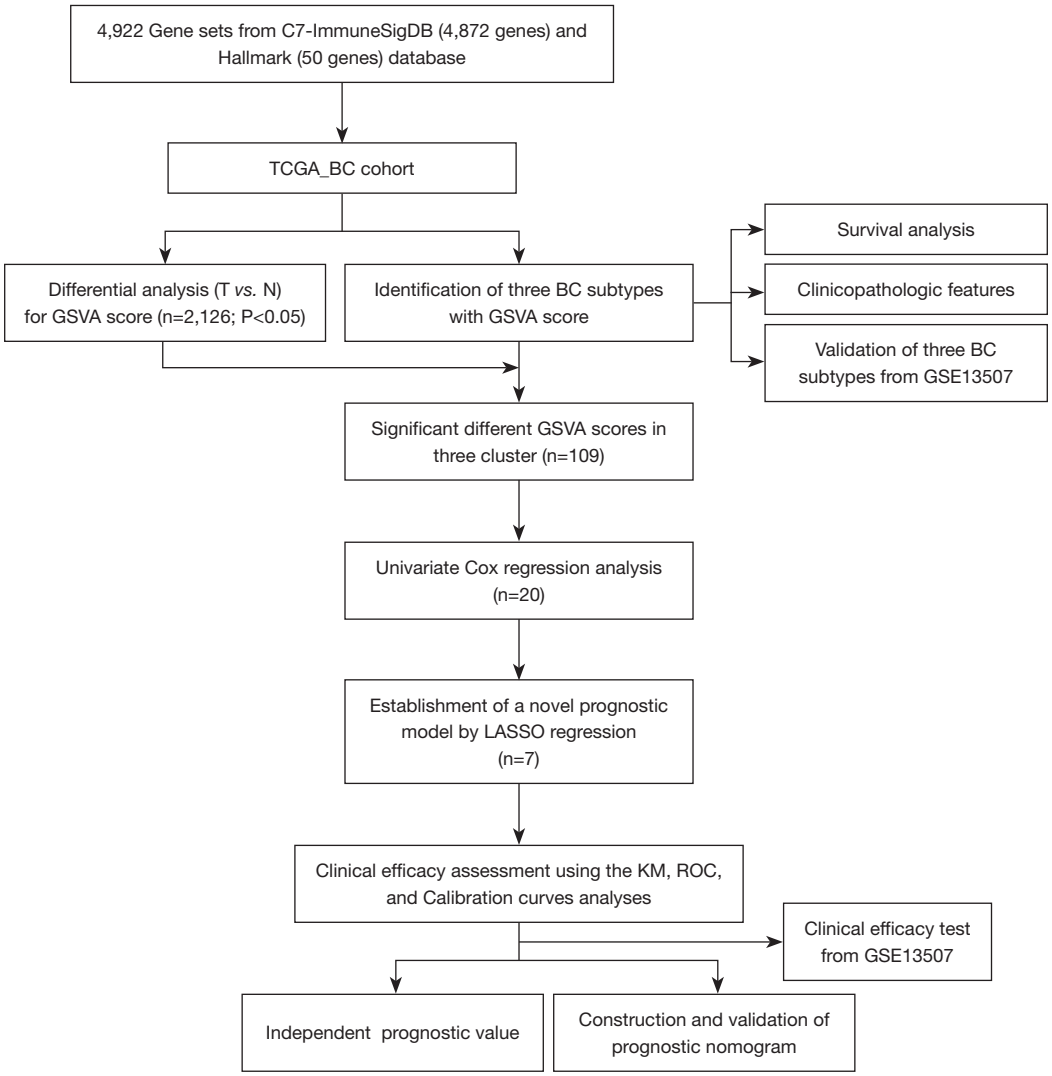

Figure 1 Flow chart of this study. GSVA, gene set variation analysis; TCGA-BC, The Cancer Genome Atlas bladder cancer; T, tumor; N, normal; BC, bladder cancer; LASSO, least absolute shrinkage and selection operator; KM, Kaplan-Meier; ROC, receiver operating characteristic.

and 19 para-cancer samples, and their clinicopathological information were downloaded from The Cancer Genome Atlas (TCGA) (https://portal.gdc.cancer.gov/projects/TCGA-BC). A total of 165 primary BC samples and their clinical characteristics were downloaded from the GEO database (https://www.ncbi.nlm.nih.gov/geo/). In total, 4,922 immunologic and hallmark gene sets were extracted from MsigDB database (http://www.gsea-msigdb.org/gsea/index.jsp) (table available at https://cdn.amegroups.cn/static/public/tcr-24-327-1.xlsx).

GSVA and clustering

The generation of a GSVA enrichment score was performed using the GSVA R package (version 1.30.0; https://bioconductor.org/packages/release/bioc/html/GSVA.html), which takes a gene-by-sample expression matrix as input and provides a gene-set-by-sample enrichment score matrix as output.

Subsequently, features were chosen through Cox regression analysis and samples were stratified into distinct

groups using the nonnegative matrix factorization (NMF) method, and the silhouette width metric was used to evaluate how accurately a sample matched the identified subtype compared to other subtypes. An additional expression profile dataset (GSE13507) with a different platform was utilized for validation purposes. Subsequent to this, the correlation between BC subtypes and clinical characteristics was assessed via chi-square test. Lastly, differential enrichment scores of gene sets were calculated between the three subtypes, intersected, and refined through Cox analysis (P<0.05) (Table S1; Table S2).

Construction of the risk score model

Subsequently, least absolute shrinkage and selection operator (LASSO) regression analysis was performed to construct a prognostic model based on the seven gene sets significantly associated with prognosis (P<0.05) (Table S3). Kaplan-Meier (KM) survival curves were utilized to assess the prognostic ability of the risk score within both TCGA and GEO cohorts. Furthermore, univariate and multivariate Cox regression analyses were performed to validate the independent prognostic value of the risk score.

Establishment and evaluation of the prognostic model

A nomogram was constructed to estimate the 1-, 3-, and 5-year overall survival (OS) of BC patients, incorporating variables such as grade, age, gender, stage, risk score, distant metastasis, and lymph node metastasis. To assess the accuracy of the nomogram, receiver operating characteristic (ROC) curve analysis was performed. Subsequently, decision curve analysis (DCA) was utilized to validate the predictive effectiveness of the prognostic model.

Gene set enrichment analysis and the identification of immune-related hub genes

On tumor (T) and normal (N) gene sets, Gene Ontology (GO) and Kyoto Encyclopedia of Genes and Genomes (KEGG) analyses were performed. GO was used to analyze the relationship of biological process (BP), cellular components (CC), and molecular function (MF) with the gene sets. KEGG analysis was used on the T and N gene sets. The differentially expressed genes involved in tumor signaling pathways and tumor progression were analyzed. The Molecular Complex Detection (MCODE) plug-in was used to explore the hub genes based on the N gene sets of the prognostic model.

Statistical analysis

Chi-squared test or Fisher's exact test was used to analyze the relationship between clinical characteristics and subtype. Univariate survival analysis was carried out with KM survival analysis. Multivariate survival analysis was performed using the Cox regression model.

Ethical statement

The study was conducted in accordance with the Declaration of Helsinki (as revised in 2013).

Results

BC subtypes based on the immune-related and hallmark gene sets

The initial step of the study involved analyzing GSVA from the TCGA-BC Cohort, encompassing 19 normal bladder tissues and 406 BC tissues (*Figure 2*). Subsequently, the CancerSubtype R package was employed for subtyping and survival analysis, based on the GSVA scores (*Figure 3A*). The optimal number of clusters, K (K=3), was quantified using the sum of squared error calculation (Figure S1A,S1B). The Silhouette method was utilized to assess intracluster cohesion and intercluster separations, with silhouette coefficients close to 1 indicating well-classified elements within a particular cluster (*Figure 3B*). A comparison of the OS among the three subtypes revealed that C1 patients exhibited a poorer prognosis compared to the other patients (P<0.05) (*Figure 3C*). This observation was also consistent with disease-specific survival (DSS) (P<0.05) and progression-free survival (PFS) (P<0.05) (*Figure 3D,3E*).

Construction and evaluation of a risk scoring model of seven immune-related gene sets among three clusters

To investigate the relationship between the differentially expressed gene sets of the three clusters and prognosis, a visual Venn diagram was utilized (*Figure 4A*). The results indicated that 109 gene sets had an impact on all three groups. The screened genomes were summarized by heatmaps, which further demonstrated their close association with the newly established genotypes (*Figure 4B*). Employing univariate Cox regression, 20 gene sets significantly associated with prognosis were identified (Table S2). Finally, seven gene sets were incorporated into a regression model using the LASSO strategy (*Figure 5A,5B*).

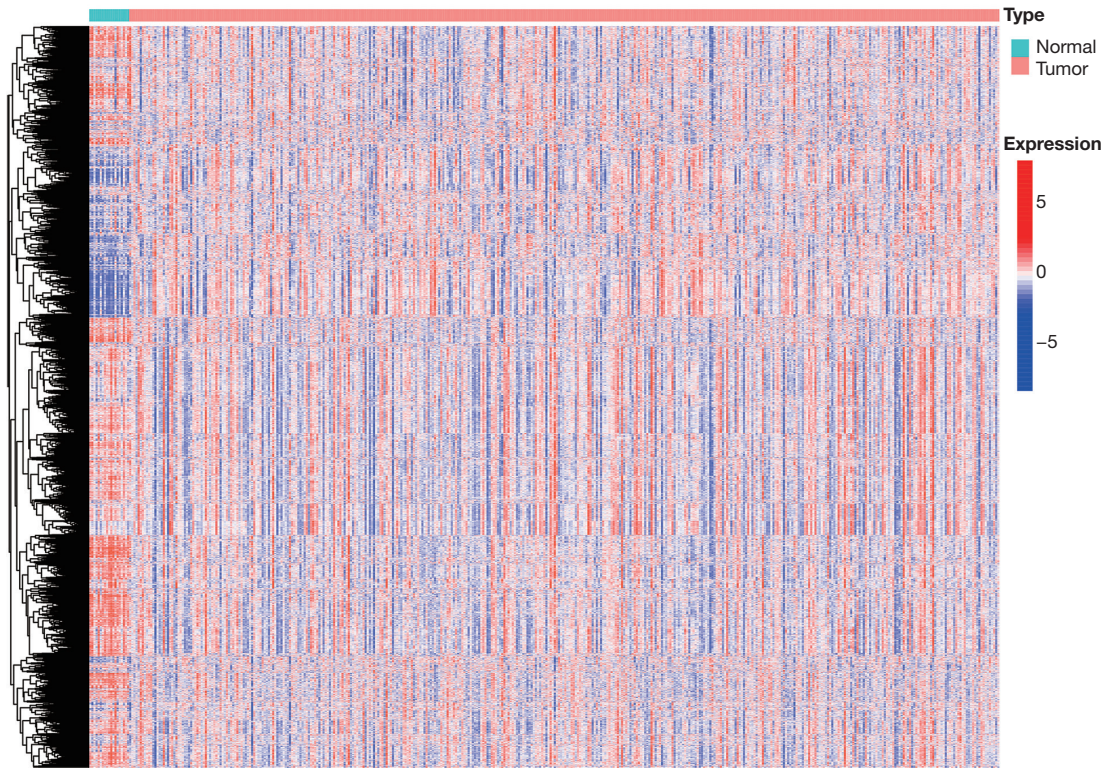

Figure 2 Heat map of GSVA enrichment scores from 4,922 immunologic and hallmark gene sets in tumor and non-tumor tissues based on TCGA-BC. GSVA, gene set variation analysis; TCGA-BC, The Cancer Genome Atlas bladder cancer.

Among these gene sets, six were in non-tumor tissues (N gene sets: N_GSE1460_CD4_THYMOCYTE_VS_THYMIC_STROMAL_CELL_DN, N_GSE26488_WT_VS_HDAC7_DELTAP_TG_OT2_THYMOCYTE_WITH_PEPTIDE_INJECTION_DN, N_HALLMARK_APICAL_JUNCTION, N_GSE1432_6H_VS_24H_IFNG_MICROGLIA_UP, N_GSE43955_1H_VS_42H_ACT_CD4_TCELL_WITH_TGFB_IL6_DN, N_HALLMARK_HYPOXIA), and one was in tumor tissues (T gene sets: T_GSE25088_WT_VS_STAT6_KO_MACROPHAGE_DN). Therefore, the gene sets of the final prognostic model and their corresponding coefficients were presented in Table S3.

Furthermore, TCGA data were used as a training set and GSE13507 data were used as a validation set. Then, we analyzed the GSE13507 dataset to classify BC patients into three different subtypes with a silhouette width value of 0.87 following the same approach as the TCGA dataset, and the BC patients with subtype1 exhibited the shortest survival time compared to patients with other subtypes (P=0.000342; Figure S2). In order to better identify patients at high and low risk, cutoff values defining low- and high-risk groups were derived by dividing the training set and the validation set risk scores into median. KM analysis revealed that the OS of patients in the low-risk group was significantly higher than that of those in the high-risk group in both the training set and the validation set (*Figure 5C,5D*), and the three prognostic gene sets in the model were strongly correlated with survival status (Figure S3). The results of calibration curve and ROC curve [TCGA training set: 1-year area under the curve (AUC) =0.654, 3-year AUC =0.643, 5-year AUC =0.647; GEO validation set: 1-year AUC =0.709, 3-year AUC =0.627, 5-year AUC =0.603] analysis all showed that our model had good prediction performance (*Figure 5E-5H*).

Establishment and evaluation of the prognostic model

A subgroup analysis revealed that the model exhibited satisfactory predictive capabilities with respect to age, gender, grading, staging, the presence of distant metastasis, and the presence of lymph node metastasis (*Figure 6A-6G*).

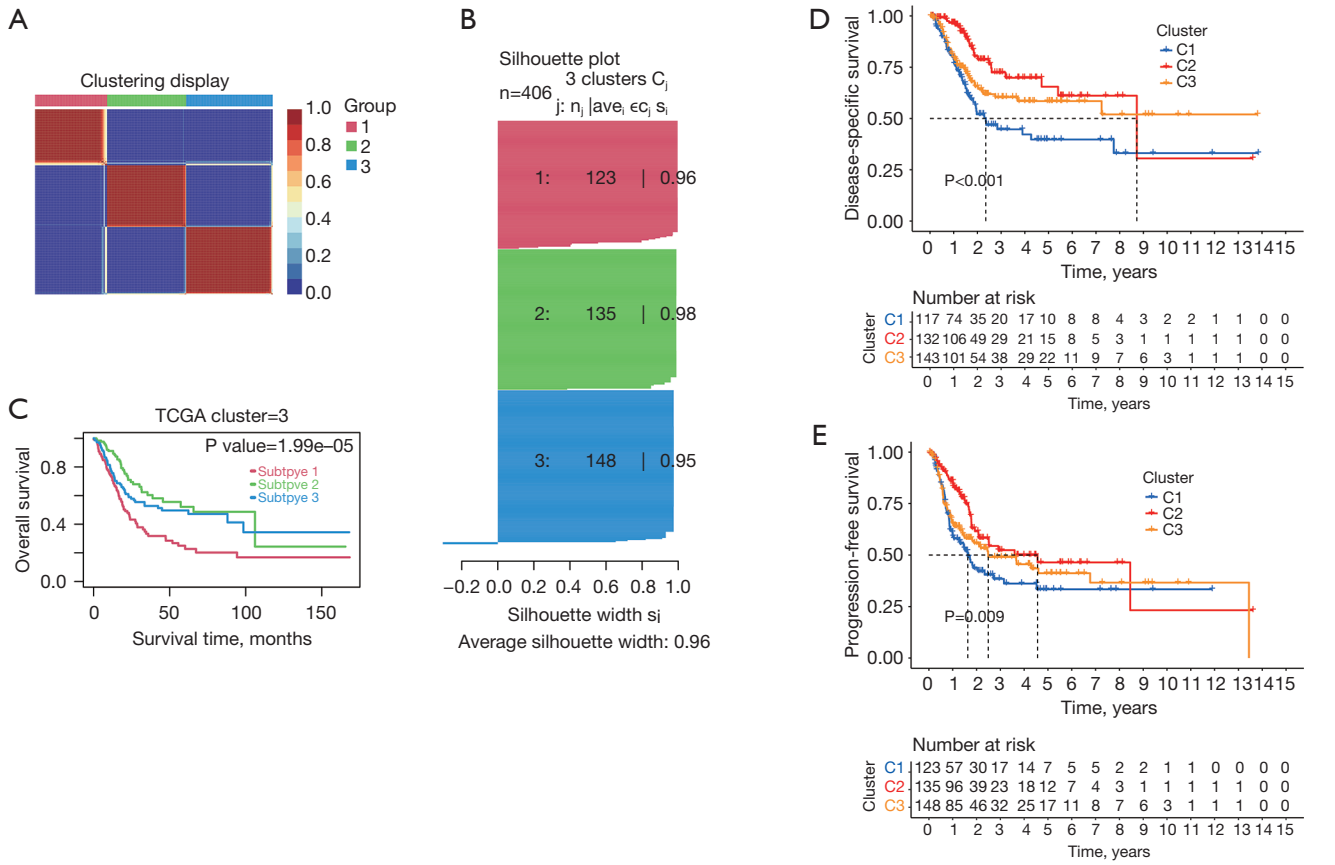

Figure 3 Identification of BC subtypes based on TCGA. (A) The NMF method was employed to cluster BC samples. (B) Silhouette width plots with an average value of 0.96. (C) KM survival curve for OS among the three subtypes. (D) KM survival analyses of DSS and (E) PFS among the three subtypes. BC, bladder cancer; TCGA, the cancer genome atlas; KM, Kaplan-Meier; OS, overall survival; NMF, nonnegative matrix factorization; DSS, disease-specific survival; PFS, progression-free survival; TCGA-BC, The Cancer Genome Atlas bladder cancer.

To evaluate the prognostic value of the risk score, univariable Cox regression analysis was performed on the training set, incorporating variables such as age, gender, grade, and stage. It was found that age, stage, and the risk score exhibited significant prognostic value (*Figure 6H*). Subsequent multivariate Cox regression analysis confirmed that the risk score could be utilized as an independent prognostic factor (*Figure 6I*). A nomogram was developed in the training set, integrating grade, age, gender, stage, risk score, distant metastasis, and lymph node metastasis, to enhance clinical applicability (*Figure 7A*). The calibration curve demonstrated that the nomogram possessed good predictive performance at 1, 3, and 5 years (*Figure 7B*), with the ROC curve analysis corroborating this finding (*Figure 7C*). DCA for 1-, 3-, and 5-year outcomes was conducted to validate the predictive efficacy of the risk score model and the nomogram (*Figure 7D-7F*).

GO and KEGG analysis on gene sets and the screening of the hub genes

In order to further investigate the functions of genes in T and N gene sets from the prognostic model, GO and KEGG analyses were performed on T and N gene sets, respectively. Results from GO analysis were observed to correspond to different functions in the T and N gene sets. Some BP GO terms, such as extracellular matrix organization and extracellular structure organization, were enriched on T sets. On N sets, organelle fission and nuclear division were significantly enriched in BP. In terms of CC, cell-cell junctions and cell-matrix junctions were enriched in the T-set, whereas chromosomal regions and

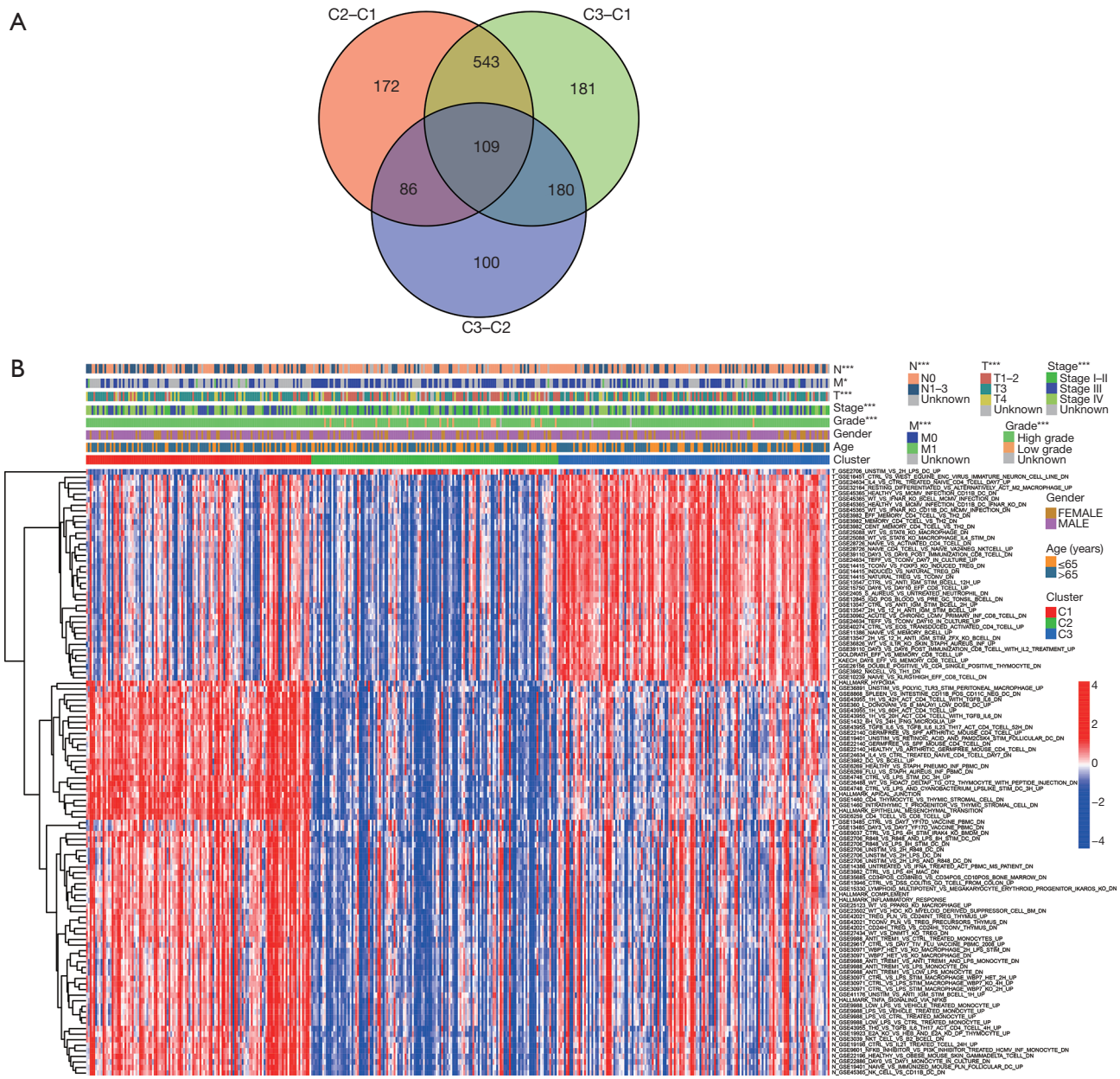

Figure 4 The representative gene sets within three subtypes. (A) Differential gene sets between each pair of subtypes were identified and intersected. (B) The heat map of 109 representative gene sets in BC subtypes, at the top, with the correlation of the three subtypes with the clinical features. *, P<0.05; ***, P<0.001. BC, bladder cancer; T, stage-T; N, stage-N; M, stage-M.

spindles were enriched in the N-set. Furthermore, several MF GO terms, such as cadherin binding, integrin binding, and glycosaminoglycan binding, were enriched on T sets (*Figure 8A*). ATPase activity, microtubule binding, and tubulin binding were enriched on N sets (*Figure 8B*). Similarly, results from KEGG on T sets showed enrichment on DNA replication and mismatch repair (*Figure 8C*). The PI3K-Akt signaling pathway showed the most significant enrichment on N sets (*Figure 8D*).

Using the Search Tool for the Retrieval of Interacting Genes/Proteins (STRING) database (https://cn.string-db.org/), protein-protein interaction (PPI) networks were constructed for genes from T and N gene sets of the model, respectively. Then, the top 10 genes with neighbors and

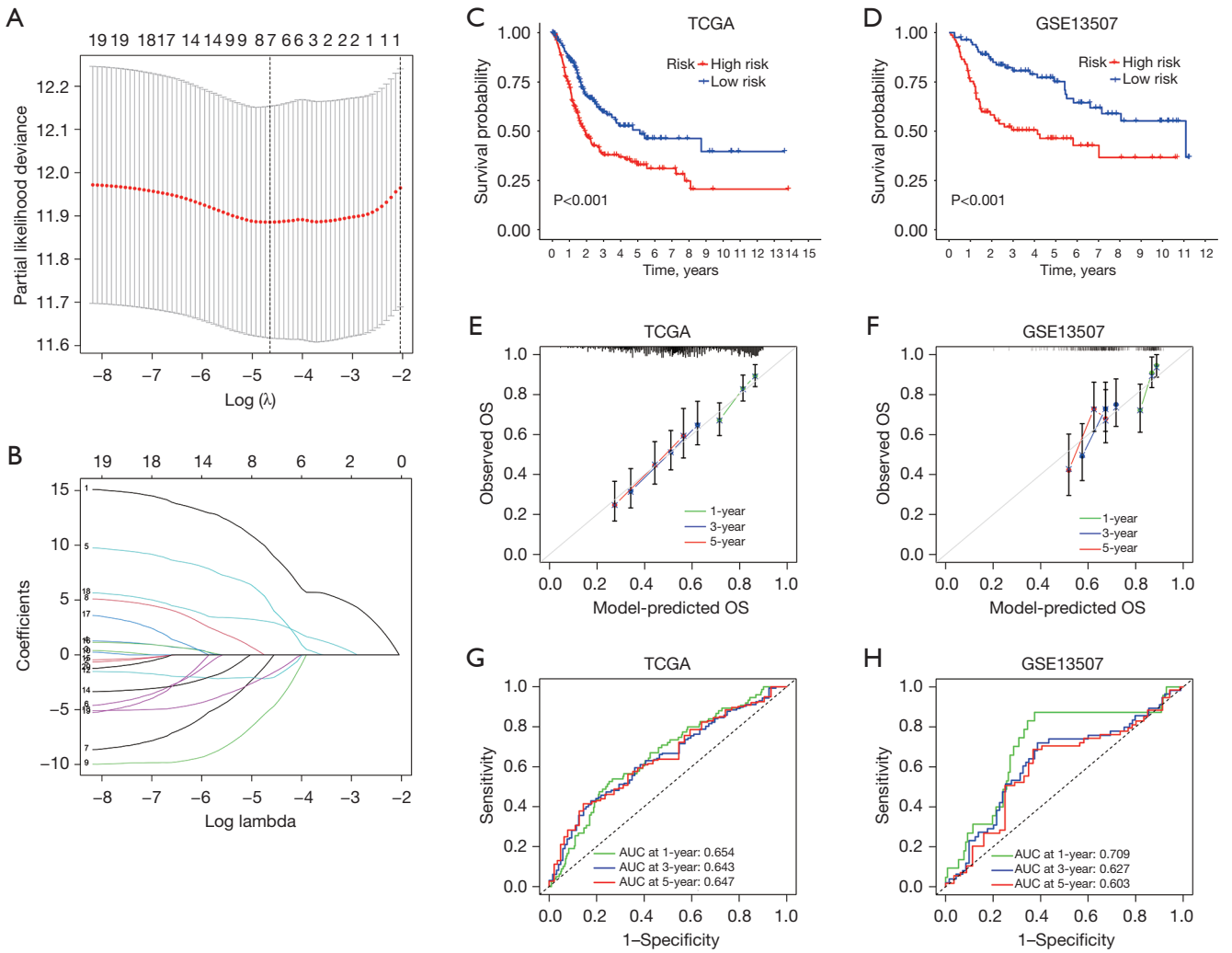

Figure 5 Establishment and validation of a risk prognostic model. (A,B) LASSO coefficient profiles via 10-fold cross validation further screened out 7 prognosis-related gene sets that were significantly related to prognosis. (C,D) Kaplan-Meier survival analyses of OS of model high- and low-risk groups from the TCGA training set and GEO test set. (E,F) The calibration curves for 1, 3, 5 years OS in the TCGA and GEO cohorts. (G,H) ROC curves for BC patients in TCGA and GEO datasets. LASSO, least absolute shrinkage and selection operator; λ, lambda; OS, overall survival; TCGA, The Cancer Genome Atlas; GEO, Gene Expression Omnibus; ROC, relative operating characteristic; AUC, area under the curve; BC, bladder cancer.

expanded genes calculated by the cytoHubba plugin in Cytoscape with highest degree, according to T and N gene sets of the model, respectively (*Figure 8E,8F*). Furthermore, an effort was made to identify subnetwork 1 (subnet1) and subnetwork 2 (subnet2) of PPI network based on the T and N gene sets of the prognostic model, which were analyzed using the MCODE plug-in. As a result, two subnetworks were obtained: subnet1, and subnet2 (Figure S4A-S4D). The deep red nodes in these subnets represent the hub genes. For instance, EGFR and ITGA2 of N gene sets were identified and considered as the critical genes.

Discussion

Predicting the prognosis of cancer accurately is crucial for guiding our treatment strategies, enabling targeted personalized treatment for patients, and facilitating appropriate review plans. MIBC is characterized by rapid progression, high metastatic potential, and poor prognosis (10). Stage and grade largely determine the

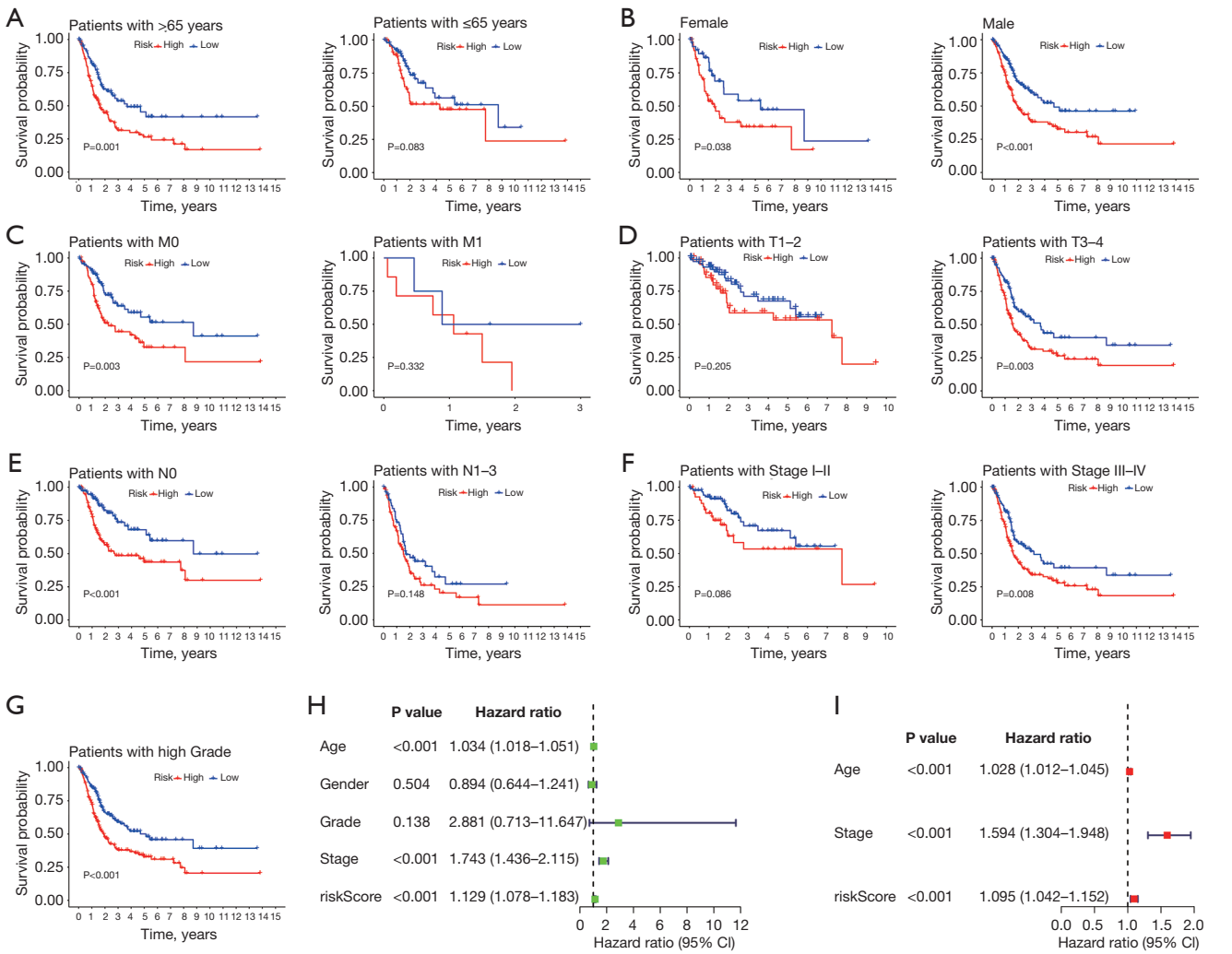

Figure 6 Clinical prognostic value of the risk model based on TCGA database. (A-G) Stratified KM analysis was conducted based on the different clinicopathological factors. (H,I) Univariate survival analysis and multivariate survival analysis of the risk model and assessment of other clinical characteristics. KM, Kaplan-Meier; T, stage-T; N, stage-N; M, stage-M; CI, confidence interval; TCGA, The Cancer Genome Atlas.

treatment of BC and significantly affect the prognosis. Currently, cancer risk is primarily determined by tumor, node, metastasis (TNM) stage and pathological diagnosis (11), yet there remains a gap in the availability of a quantitative risk scoring and prediction model that is stable, accurate, and capable of rapid assessment. As research advances, the ICB revolution has brought hope to patients with advanced BC (12). The treatment of ICB is mainly related to the TME (13), which includes all noncancerous host cells, extracellular matrix (ECM), and soluble products in the tumor, where many immune-related genes are present (14). Emerging evidence suggests that the presence of tertiary lymphoid structures (TLS) and neutrophil to lymphocyte ratio (NLR) in peripheral blood is associated with the treatment response to checkpoint inhibitors (CPIs). Specifically, patients with metastatic urothelial carcinoma (mUC) who have lower NLR and exhibit TLS in their tumors show significantly improved OS and PFS when treated with pembrolizumab, compared to those without TLS. This suggests that both TLS and NLR are important biomarkers for predicting CPI efficacy (15). Additionally, alterations in *FGFR3* (aFGFR3) in BC have been found to impact the TME and the efficacy of immune checkpoint inhibitors (ICIs), particularly in MIBC. Patients with the

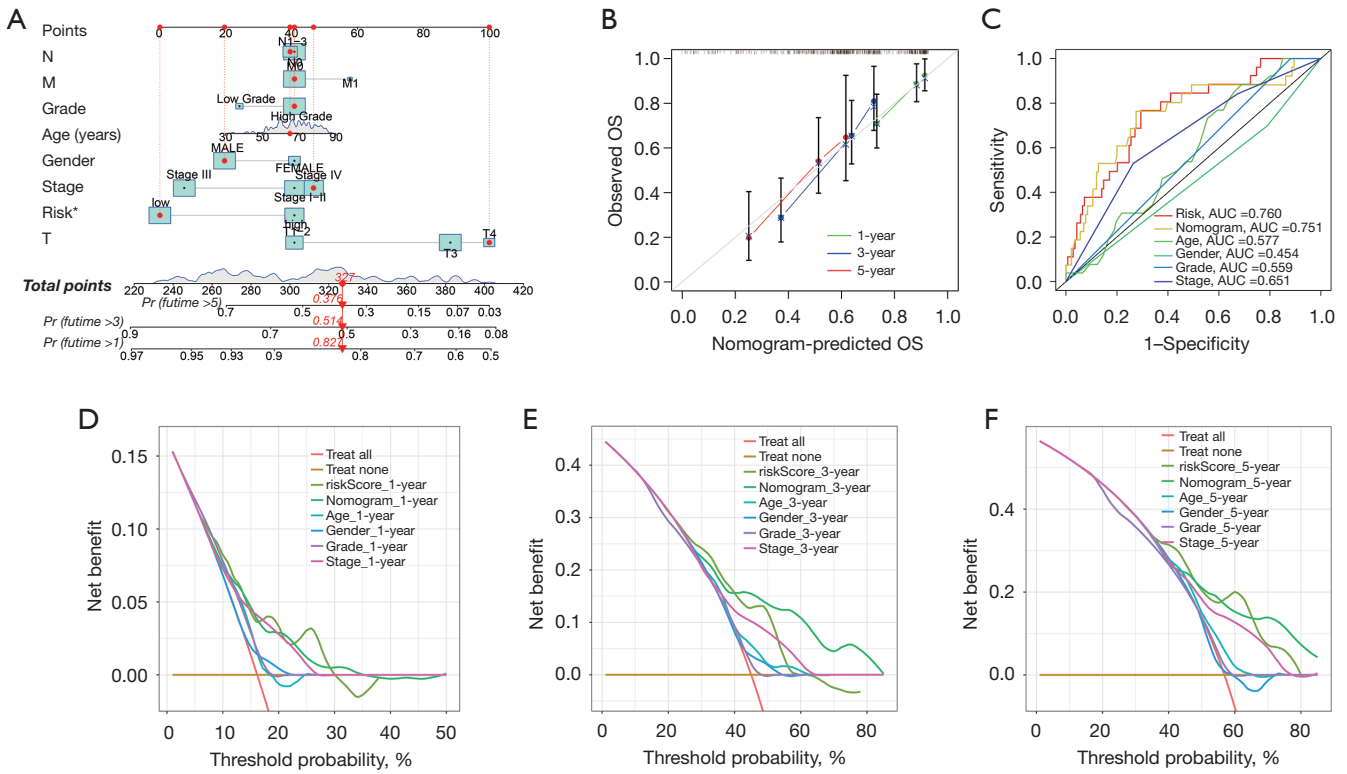

Figure 7 The nomogram was developed and validated from the TCGA database. (A) Prognosis nomogram including risk scores and clinicopathological stages was developed to forecast prognosis in BC patients. (B) Nomogram calibration curves over 1-, 3-, and 5-years. (C) 1-year ROC curves of the risk score and other clinical features. (D-F) Decision curve analysis of the OS-related nomogram at 1-, 3-, and 5-year. *, P<0.05. TCGA, The Cancer Genome Atlas; BC, bladder cancer; ROC, relative operating characteristic; OS, overall survival; T, stage-T; N, stage-N; M, stage-M; Pr, probability; Futime, survival time; AUC, area under the curve.

LumP subtype harboring aFGFR3 show a higher objective response rate to immune therapy compared to those with intact FGFR3 (iFGFR3) (16).

Consequently, the design of a prognostic model enabled the utilization of the immune-related genome to inform the treatment of BC and identify novel immunotherapeutic targets that are anticipated to be developed and applied in the future. After KM survival analysis, the low-risk group exhibited superior survival outcomes compared to the high-risk group. This model demonstrates stronger predictive efficacy, particularly among patients with advanced stage BC, characterized by a high degree of malignancy. Subsequently, the nomogram visually illustrates the prediction effect of the model. Furthermore, the calibration curve, ROC curve, and DCA were employed to verify the accuracy and reliability of the model.

GO enrichment analysis revealed that ECM organization is associated with the N gene set in the model. As a critical component of TME, ECM interacts with cytokines, chemokines, and cancer cells to construct a cross-linking signaling network (17). A previous study has shown that remodeling of ECM is associated with the promotion of malignant tumor development and poor patient prognosis (18). Through KEGG enrichment analysis, we found that the gene sets enriched in BC adjacent tissues were highly correlated with the PI3K-Akt signaling pathway. The PI3K-Akt signaling pathway is one of the most commonly dysregulated pathways in cancer (19). It has been demonstrated that TEAD4 contributes to epithelial-mesenchymal transition (EMT) in BC cells by activating the PI3K/AKT pathway (20). Akt methylation is a crucial step that synergizes with PI3K signaling to control Akt activation, and targeting SETDB1 signaling may be a potential therapeutic strategy against overactive AkT-driven cancers (21). Additionally, immune metabolism plays a pivotal role in immunity, and it is noteworthy that the phosphoinositide 3-kinase (PI3K)-protein kinase B (AKT)-mammalian target of rapamycin (mTOR) pathway

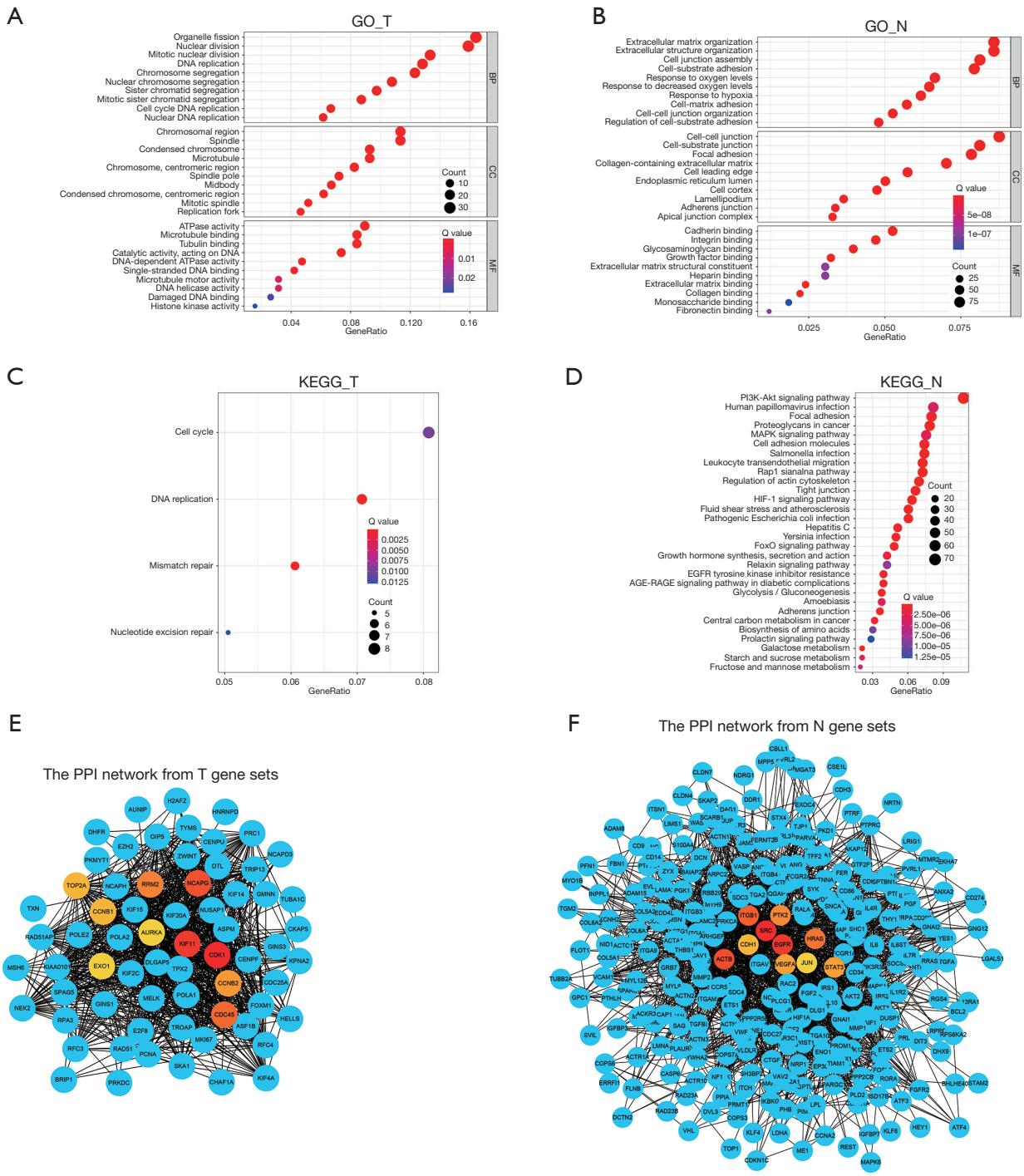

Figure 8 Analyses of GO, KEGG enrichment, PPI network for genes from T and N gene sets of the model. (A,B) GO term analysis for genes from T and N gene sets of the model, respectively. (C,D) KEGG pathway analysis for genes from T and N gene sets of the model, respectively. (E,F) The top 10 hub genes of the highest degree with neighbors and expanded genes were identified by the STRING analysis, the cytoHubba plugin in cytoscape, based on T and N gene sets of the model. GO, Gene Ontology; KEGG, Kyoto Encyclopedia of Genes and Genomes; PPI, protein-protein interaction; STRING, Search Tool for the Retrieval of Interacting Genes/Proteins; T, tumor; N, normal; BP, biological process; CC, cellular component; MF, molecular function. The colorful nodes represented 10 hub genes with the most edges, deeper color indicates higher connectivity values.

is indispensable for modulating immune functions (22). Furthermore, this pathway serves as a vital signaling mechanism underlying T cell activation and functionality (23), with the mTOR node at the core of its downstream signaling cascade emerging as a crucial regulator of immune response (24). The PI3K-Akt pathway exhibits a tight correlation with cancer hallmarks. Previous investigations have demonstrated that the PI3K-Akt pathway plays a pivotal role in the polarization, proliferative capacity, and survival mechanisms of M2-like tumor-associated macrophages. Subsequently, this pathway is implicated in promoting tumor growth, facilitating metastasis, initiating tissue remodeling processes, and inducing immunosuppressive effects (25). Furthermore, DNA-binding 2 inhibitors are also capable of suppressing the progression and metastasis of BC via the PI3K-Akt signaling pathway (26). Although inhibitors of this signaling pathway exhibit some cytotoxicity and resistance, current combination therapy, including PI3K/Akt/mTOR inhibitors, has been utilized to improve patient response and clinical outcomes. In conclusion, PI3K-Akt can be considered a promising prognostic factor and therapeutic target in BC.

An increasing number of studies have demonstrated the efficacy of ICIs in treating BC, albeit most BC patients show no sensitivity towards these present therapeutic targets. Therefore, there is a pressing need to identify novel prognostic biomarkers and predictors of treatment response to promote individualized and precise treatment of BC. Within the N gene set, *EGFR* and *ITGA2* were identified as two pivotal genes owing to their high degree values. In the context of cancer metastasis, exosome-mediated signaling factors play a pivotal role in activating the epidermal growth factor receptor (EGFR) signaling pathway, thereby contributing significantly to the progression of cancer metastasis (27). Monoclonal antibodies or small molecule tyrosine kinase inhibitors (TKIs) targeting EGFR inhibition have been approved for treating RAS wild-type colorectal cancer (28), and have also been shown to be beneficial in basal-like MIBC (29). The *EGFR* gene is also intricately linked to anti-tumor immunity, and the abnormal activation of the EGFR signaling pathway can occur in conjunction with the PI3K/AKT/mTOR and p53 signaling pathways. This interaction regulates the growth and migration of tumor cells, underscoring the significance of EGFR in the context of tumorigenesis (30). Meanwhile, the upregulation of epiregulin (ERPG) primarily serves to activate the EGFR signaling pathway, thereby fostering the advancement of numerous malignancies (31). EGFR thus has promising potential for treatment of BC, a fact reinforced by this study.

ITGA2 could be a key regulatory factor in controlling the migration, invasion, and metastasis of tumor cells (32). In the conduct of this research, the immune gene set was scored utilizing MCODE methodology to search for crucial genes and *ITGA2* was identified as a significant hub gene in the adjacent tissues of bladder tumors. Although BC immunotherapy-based drugs and clinical trials targeting ITGA2 have yet to be developed, previous findings indicate that ITGA2 has a role in cancer development. Studies have shown that ITGA2 is abnormally overexpressed and significantly associated with poor survival of several malignant tumors (32,33). Research has conclusively demonstrated a positive correlation between the expression of ITGA2 and programmed cell death ligand 1 (PD-L1) within the pancreatic cancer TME. In addition, the inhibition of ITGA2 has been shown to effectively attenuate the proliferative and invasive capabilities of pancreatic cancer cells (34). Blocking ITGA2 improves tumor immune response by reducing the phosphorylation level of STAT3 and inhibiting PD-L1 expression *in vivo* (35). Overall, ITGA2 may serve as a novel prognostic biomarker for BC and a new target for ICB therapy.

The gene set variation analysis (GSVA) score-based predictive model provides a novel perspective for constructing prognostic models for bladder tumors. As tools for predicting patient prognosis continue to develop, the potential for future advancements remains promising. The integration of artificial intelligence (AI) and radiomics into healthcare is expected to significantly enhance the management of BC. AI-driven algorithms, leveraging extensive datasets, are anticipated to improve predictive accuracy and clinical outcomes (36). Furthermore, AI and radiomics can aid in distinguishing benign from malignant lesions and predicting treatment responses in metastatic renal cell carcinoma, thereby enhancing diagnostic precision (37). Additionally, patient demographics, such as age, play a crucial role in prognosis. For instance, older patients with BC face higher risks of recurrence and progression, emphasizing the necessity for personalized treatment strategies (38). Future research should focus on refining these technologies to achieve more precise and individualized therapeutic approaches, providing new hope and improved outcomes for BC patients. Integrating existing methods with multidimensional information will offer the most effective tools for accurately predicting patient prognosis and guiding treatment.

Conclusions

These findings provide important insights for the development of new ICB therapies for BC treatment. In summary, the research comprehensively examined alterations in hallmark and immunologic gene sets and developed an innovative prognostic model for risk stratification in BC, offering a fresh approach to enhancing prognostic evaluation methods in subsequent studies. Additionally, the study identified several potential immunotherapy targets for BC, such as the PI3K-Akt signaling pathway, *EGFR*, and *ITGA2*.

Acknowledgments

We sincerely thank all participants in the study.

Funding: The present study was supported by Tianjin Municipal Health Industry Key Project (No. TJWJ2022XK014), Scientific Research Project of Tianjin Municipal Education Commission (No. 2022ZD069), Tianjin Institute of Urology Talent Funding Program (No. MYSRC202310), the Youth Fund of Tianjin Medical University Second Hospital (No. 2022ydey15), and The Talents Cultivated Project of Department of Urology, the Second Hospital of Tianjin Medical University (No. MNRC202313).

Footnote

Reporting Checklist: The authors have completed the TRIPOD reporting checklist. Available at https://tcr.amegroups.com/article/view/10.21037/tcr-24-327/rc

Peer Review File: Available at https://tcr.amegroups.com/article/view/10.21037/tcr-24-327/prf

Conflicts of Interest: All authors have completed the ICMJE uniform disclosure form (available at https://tcr.amegroups.com/article/view/10.21037/tcr-24-327/coif). The authors have no conflicts of interest to declare.

Ethical Statement: The authors are accountable for all aspects of the work in ensuring that questions related to the accuracy or integrity of any part of the work are appropriately investigated and resolved. The study was conducted in accordance with the Declaration of Helsinki (as revised in 2013).

References

1. Wu X, Lv D, Cai C, et al. A TP53-Associated Immune Prognostic Signature for the Prediction of Overall Survival and Therapeutic Responses in Muscle-Invasive Bladder Cancer. Front Immunol 2020;11:590618.
2. Yan S, Zeng H, Jin K, et al. NKG2A and PD-L1 expression panel predicts clinical benefits from adjuvant chemotherapy and PD-L1 blockade in muscle-invasive bladder cancer. J Immunother Cancer 2022;10:e004569.
3. Ferlay J, Colombet M, Soerjomataram I, et al. Estimating the global cancer incidence and mortality in 2018: GLOBOCAN sources and methods. Int J Cancer 2019;144:1941-53.
4. Witjes JA, Bruins HM, Cathomas R, et al. European Association of Urology Guidelines on Muscle-invasive and Metastatic Bladder Cancer: Summary of the 2020 Guidelines. Eur Urol 2021;79:82-104.
5. Balar AV, Galsky MD, Rosenberg JE, et al. Atezolizumab as first-line treatment in cisplatin-ineligible patients with locally advanced and metastatic urothelial carcinoma: a single-arm, multicentre, phase 2 trial. Lancet 2017;389:67-76.
6. Apolo AB, Infante JR, Balmanoukian A, et al. Avelumab, an Anti-Programmed Death-Ligand 1 Antibody, In Patients With Refractory Metastatic Urothelial Carcinoma: Results From a Multicenter, Phase Ib Study. J Clin Oncol 2017;35:2117-24.
7. Sharma P, Retz M, Siefker-Radtke A, et al. Nivolumab in metastatic urothelial carcinoma after platinum therapy (CheckMate 275): a multicentre, single-arm, phase 2 trial. Lancet Oncol 2017;18:312-22.
8. Sun Y, Sedgwick AJ, Khan MA, et al. A Transcriptional Signature of IL-2 Expanded Natural Killer Cells Predicts More Favorable Prognosis in Bladder Cancer. Front Immunol 2021;12:724107.
9. Cao M, Cao Y, Xue S, et al. Therapeutic Benefits and Prognostic Value of a Model Based on 7 Immune-associated Genes in Bladder Cancer. Altern Ther Health

Med 2024;30:130-8.
10. Kulkarni GS, Black PC, Sridhar SS, et al. Canadian Urological Association guideline: Muscle-invasive bladder cancer. Can Urol Assoc J 2019;13:230-8.
11. Zheng Z, Lai C, Li W, et al. Identification of a Novel Glycolysis-Related LncRNA Signature for Predicting Overall Survival in Patients With Bladder Cancer. Front Genet 2021;12:720421.
12. Rijnders M, de Wit R, Boormans JL, et al. Systematic Review of Immune Checkpoint Inhibition in Urological Cancers. Eur Urol 2017;72:411-23.
13. Hu J, Yu A, Othmane B, et al. Siglec15 shapes a non-inflamed tumor microenvironment and predicts the molecular subtype in bladder cancer. Theranostics 2021;11:3089-108.
14. Xiao Y, Yu D. Tumor microenvironment as a therapeutic target in cancer. Pharmacol Ther 2021;221:107753.
15. Komura K, Tokushige S, Ishida M, et al. Tertiary lymphoid structure and neutrophil-lymphocyte ratio coordinately predict outcome of pembrolizumab. Cancer Sci 2023;114:4622-31.
16. Komura K, Hirosuna K, Tokushige S, et al. The Impact of FGFR3 Alterations on the Tumor Microenvironment and the Efficacy of Immune Checkpoint Inhibitors in Bladder Cancer. Mol Cancer 2023;22:185.
17. Mao X, Xu J, Wang W, et al. Crosstalk between cancer-associated fibroblasts and immune cells in the tumor microenvironment: new findings and future perspectives. Mol Cancer 2021;20:131.
18. Saint A, Van Obberghen-Schilling E. The role of the tumor matrix environment in progression of head and neck cancer. Curr Opin Oncol 2021;33:168-74.
19. Song Y, Guerrero-Juarez CF, Chen Z, et al. The Msi1-mTOR pathway drives the pathogenesis of mammary and extramammary Paget's disease. Cell Res 2020;30:854-72.
20. Chi M, Liu J, Mei C, et al. TEAD4 functions as a prognostic biomarker and triggers EMT via PI3K/AKT pathway in bladder cancer. J Exp Clin Cancer Res 2022;41:175.
21. Guo J, Dai X, Laurent B, et al. AKT methylation by SETDB1 promotes AKT kinase activity and oncogenic functions. Nat Cell Biol 2019;21:226-37.
22. Chou WC, Rampanelli E, Li X, et al. Impact of intracellular innate immune receptors on immunometabolism. Cell Mol Immunol 2022;19:337-51.
23. Herrero-Sánchez MC, Rodríguez-Serrano C, Almeida J, et al. Targeting of PI3K/AKT/mTOR pathway to inhibit T cell activation and prevent graft-versus-host disease development. J Hematol Oncol 2016;9:113.
24. Mafi S, Mansoori B, Taeb S, et al. mTOR-Mediated Regulation of Immune Responses in Cancer and Tumor Microenvironment. Front Immunol 2022;12:774103.
25. Yang D, Yang L, Cai J, et al. Phosphoinositide 3-kinase/Akt and its related signaling pathways in the regulation of tumor-associated macrophages polarization. Mol Cell Biochem 2022;477:2469-80.
26. Mao W, Wang K, Sun S, et al. ID2 Inhibits Bladder Cancer Progression and Metastasis via PI3K/AKT Signaling Pathway. Front Cell Dev Biol 2021;9:738364.
27. Fares J, Fares MY, Khachfe HH, et al. Molecular principles of metastasis: a hallmark of cancer revisited. Signal Transduct Target Ther 2020;5:28.
28. Lièvre A, Bachet JB, Le Corre D, et al. KRAS mutation status is predictive of response to cetuximab therapy in colorectal cancer. Cancer Res 2006;66:3992-5.
29. Rose M, Maurer A, Wirtz J, et al. EGFR activity addiction facilitates anti-ERBB based combination treatment of squamous bladder cancer. Oncogene 2020;39:6856-70.
30. Zhang X, Ma H, Gao Y, et al. The Tumor Microenvironment: Signal Transduction. Biomolecules 2024;14:438.
31. Cheng WL, Feng PH, Lee KY, et al. The Role of EREG/EGFR Pathway in Tumor Progression. Int J Mol Sci 2021;22:12828.
32. Gong J, Lu X, Xu J, et al. Coexpression of UCA1 and ITGA2 in pancreatic cancer cells target the expression of miR-107 through focal adhesion pathway. J Cell Physiol 2019;234:12884-96.
33. Cai H, Guo F, Wen S, et al. Overexpressed integrin alpha 2 inhibits the activation of the transforming growth factor β pathway in pancreatic cancer via the TFCP2-SMAD2 axis. J Exp Clin Cancer Res 2022;41:73.
34. Jin L, Duan Y, Li X, et al. High expression ITGA2 affects the expression of MET, PD-L1, CD4 and CD8 with the immune microenvironment in pancreatic cancer patients. Front Immunol 2023;14:1209367.
35. Ren D, Zhao J, Sun Y, et al. Overexpressed ITGA2 promotes malignant tumor aggression by up-regulating PD-L1 expression through the activation of the STAT3 signaling pathway. J Exp Clin Cancer Res 2019;38:485.
36. Ferro M, Falagario UG, Barone B, et al. Artificial Intelligence in the Advanced Diagnosis of Bladder Cancer-Comprehensive Literature Review and Future Advancement. Diagnostics (Basel) 2023;13:2308.
37. Ferro M, Crocetto F, Barone B, et al. Artificial intelligence and radiomics in evaluation of kidney lesions:

a comprehensive literature review. Ther Adv Urol 2023;15:17562872231164803.
38. Ferro M, Chiujdea S, Musi G, et al. Impact of Age on Outcomes of Patients With Pure Carcinoma In Situ of the Bladder: Multi-Institutional Cohort Analysis. Clin Genitourin Cancer 2022;20:e166-72.

Cite this article as: Zhou X, Liu Y, Lv Z, Shen C, Yang S, Zhang Z, Tan M, Hu H. Construction and verification of an innovative immune-related and hallmark gene sets prognostic model for bladder cancer. Transl Cancer Res 2024;13(9):4639-4653. doi: 10.21037/tcr-24-327

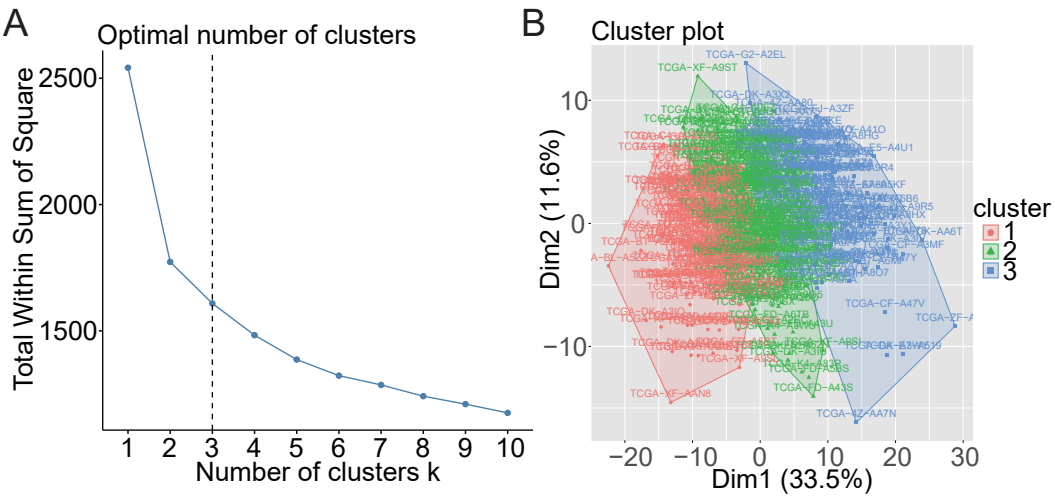

Figure S1 Identification of BC subtypes from TCGA. (A) The ideal number of clusters (K) was 3. (B) Cluster plot of 3 subtypes. BC, bladder cancer; TCGA, The Cancer Genome Atlas; Dim1, dimension 1; Dim2, Dimension 2.

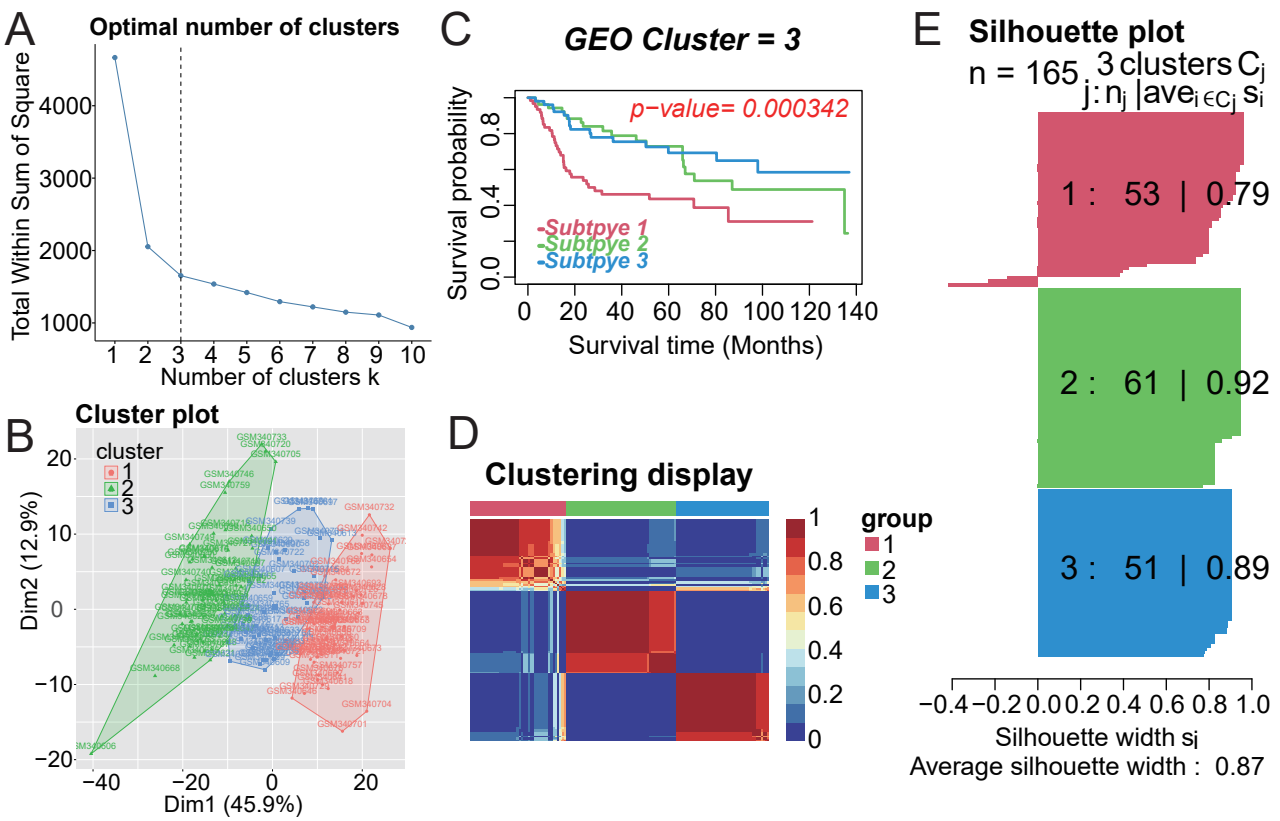

Figure S2 Identification of BC subtypes from GSE13507 was conducted. (A) The optimal number of clusters (K) was determined to be 3. (B) Visualization of the cluster results was performed. (C) Kaplan-Meier survival analysis for the three subtypes. (D) The NMF method was used to cluster BC samples. (E) Silhouette plot plots with a value of 0.87. BC, bladder cancer; NMF, nonnegative matrix factorization; GEO, gene expression omnibus; Dim1, dimension 1; Dim2, Dimension 2.

https://dx.doi.org/10.21037/tcr-24-327

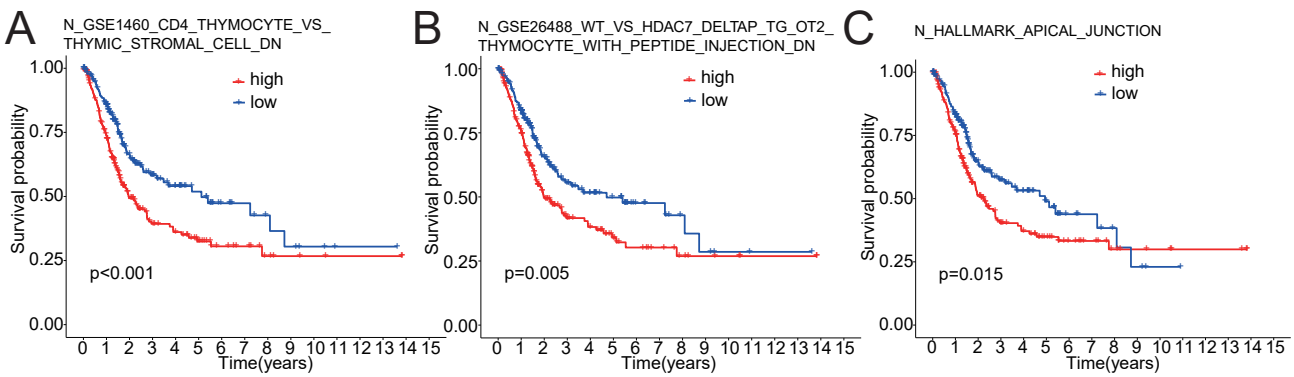

Figure S3 Kaplan-Meier survival analysis based on OS was performed for three prognostic gene sets in the model separately. OS, overall survival.

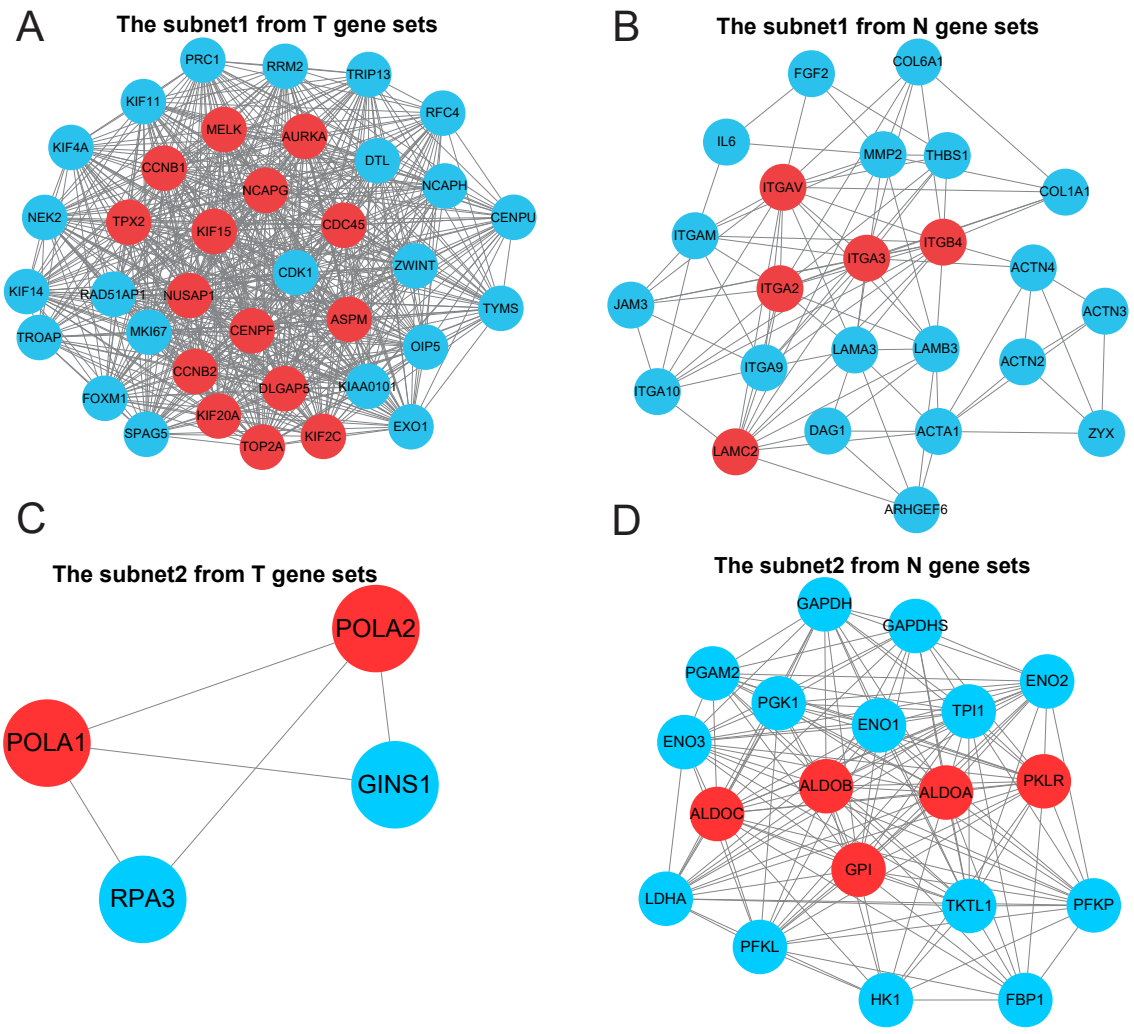

Figure S4 The (A,B) subnet1 and (C,D) subnet2 of PPI network by Cytoscape plugin MCODE of T and N gene sets. Red nodes indicate the hub genes. PPI, protein-protein interaction; MCODE, Molecular Complex Detection; T, tumor; N, normal; Subnet1, subnetwork 1; Subnet2, subnetwork 2.

https://dx.doi.org/10.21037/tcr-24-327

Table S1 The 109 differentially expressed gene sets were identified among three BC subtypes

N_GSE1460_CD4_THYMOCYTE_VS_THYMIC_STROMAL_CELL_DN
N_HALLMARK_EPITHELIAL_MESENCHYMAL_TRANSITION
N_GSE6259_CD4_TCELL_VS_CD8_TCELL_UP
N_GSE1460_INTRATHYMIC_T_PROGENITOR_VS_THYMIC_STROMAL_CELL_DN
N_GSE26488_WT_VS_HDAC7_DELTAP_TG_OT2_THYMOCYTE_WITH_PEPTIDE_INJECTION_DN
N_GSE4748_CTRL_VS_LPS_AND_CYANOBACTERIUM_LPSLIKE_STIM_DC_3H_UP
N_HALLMARK_APICAL_JUNCTION
N_GSE4748_CTRL_VS_LPS_STIM_DC_3H_UP
N_GSE1432_6H_VS_24H_IFNG_MICROGLIA_UP
N_GSE43955_1H_VS_20H_ACT_CD4_TCELL_WITH_TGFB_IL6_DN
N_GSE8868_SPLEEN_VS_INTESTINE_CD11B_POS_CD11C_NEG_DC_DN
N_GSE3982_DC_VS_BCELL_UP
N_GSE43955_1H_VS_42H_ACT_CD4_TCELL_WITH_TGFB_IL6_DN
N_GSE360_L_DONOVANI_VS_B_MALAYI_LOW_DOSE_DC_UP
N_HALLMARK_HYPOXIA
N_GSE43955_1H_VS_60H_ACT_CD4_TCELL_UP
N_GSE6269_HEALTHY_VS_STAPH_PNEUMO_INF_PBMC_DN
N_GSE6269_FLU_VS_STAPH_AUREUS_INF_PBMC_DN
N_GSE43955_TGFB_IL6_VS_TGFB_IL6_IL23_TH17_ACT_CD4_TCELL_52H_DN
T_GSE2706_UNSTIM_VS_2H_LPS_DC_UP
N_GSE19401_UNSTIM_VS_RETINOIC_ACID_AND_PAM2CSK4_STIM_FOLLICULAR_DC_DN
N_GSE22140_GERMFREE_VS_SPF_MOUSE_CD4_TCELL_DN
N_GSE24634_IL4_VS_CTRL_TREATED_NAIVE_CD4_TCELL_DAY7_DN
N_GSE2706_R848_VS_R848_AND_LPS_8H_STIM_DC_DN
N_GSE22196_HEALTHY_VS_OBESE_MOUSE_SKIN_GAMMADELTA_TCELL_DN
N_GSE9037_CTRL_VS_LPS_4H_STIM_IRAK4_KO_BMDM_DN
N_GSE22140_HEALTHY_VS_ARTHRITIC_GERMFREE_MOUSE_CD4_TCELL_DN
N_GSE19198_CTRL_VS_IL21_TREATED_TCELL_24H_UP
N_GSE19401_NAIVE_VS_IMMUNIZED_MOUSE_PLN_FOLLICULAR_DC_UP
N_GSE43955_TH0_VS_TGFB_IL6_TH17_ACT_CD4_TCELL_4H_UP
N_GSE9601_NFKB_INHIBITOR_VS_PI3K_INHIBITOR_TREATED_HCMV_INF_MONOCYTE_DN
N_GSE22140_GERMFREE_VS_SPF_ARTHRITIC_MOUSE_CD4_TCELL_UP
N_GSE3039_NKT_CELL_VS_B2_BCELL_DN
N_GSE9988_ANTI_TREM1_VS_CTRL_TREATED_MONOCYTES_UP
N_GSE36891_UNSTIM_VS_POLYIC_TLR3_STIM_PERITONEAL_MACROPHAGE_UP
N_GSE42021_CD24HI_TREG_VS_CD24HI_TCONV_THYMUS_DN
N_GSE27434_WT_VS_DNMT1_KO_TREG_DN

Table S1 (*continued*)

https://dx.doi.org/10.21037/tcr-24-327

Table S1 (*continued*)

N_GSE30971_CTRL_VS_LPS_STIM_MACROPHAGE_WBP7_KO_4H_UP
N_GSE45365_NK_CELL_VS_CD11B_DC_DN
N_GSE22886_DAY0_VS_DAY1_MONOCYTE_IN_CULTURE_DN
N_GSE19923_E2A_KO_VS_HEB_AND_E2A_KO_DP_THYMOCYTE_UP
N_GSE30971_CTRL_VS_LPS_STIM_MACROPHAGE_WBP7_HET_2H_UP
N_GSE42021_TREG_PLN_VS_CD24INT_TREG_THYMUS_UP
N_GSE2706_R848_VS_LPS_8H_STIM_DC_DN
N_GSE13946_CTRL_VS_DSS_COLITIS_GD_TCELL_FROM_COLON_UP
N_GSE25123_WT_VS_PPARG_KO_MACROPHAGE_UP
N_GSE30971_CTRL_VS_LPS_STIM_MACROPHAGE_WBP7_KO_2H_UP
N_HALLMARK_COMPLEMENT
N_HALLMARK_INFLAMMATORY_RESPONSE
N_HALLMARK_TNFA_SIGNALING_VIA_NFKB
N_GSE42021_TCONV_PLN_VS_TREG_PRECURSORS_THYMUS_DN
N_GSE23502_WT_VS_HDC_KO_MYELOID_DERIVED_SUPPRESSOR_CELL_BM_DN
N_GSE30971_WBP7_HET_VS_KO_MACROPHAGE_2H_LPS_STIM_DN
N_GSE30971_WBP7_HET_VS_KO_MACROPHAGE_DN
N_GSE2706_UNSTIM_VS_2H_R848_DC_DN
N_GSE15330_LYMPHOID_MULTIPOTENT_VS_MEGAKARYOCYTE_ERYTHROID_PROGENITOR_IKAROS_KO_DN
N_GSE14386_UNTREATED_VS_IFNA_TREATED_ACT_PBMC_MS_PATIENT_DN
N_GSE41176_UNSTIM_VS_ANTI_IGM_STIM_BCELL_1H_UP
N_GSE29617_CTRL_VS_DAY7_TIV_FLU_VACCINE_PBMC_2008_UP
N_GSE3982_CTRL_VS_LPS_4H_MAC_DN
N_GSE9988_LPS_VS_CTRL_TREATED_MONOCYTE_UP
N_GSE2706_UNSTIM_VS_2H_LPS_DC_DN
N_GSE35685_CD34POS_CD38NEG_VS_CD34POS_CD10POS_BONE_MARROW_DN
N_GSE9988_LOW_LPS_VS_VEHICLE_TREATED_MONOCYTE_UP
N_GSE9988_LOW_LPS_VS_CTRL_TREATED_MONOCYTE_UP
N_GSE9988_ANTI_TREM1_VS_LPS_MONOCYTE_DN
N_GSE9988_LPS_VS_VEHICLE_TREATED_MONOCYTE_UP
N_GSE9988_ANTI_TREM1_VS_LOW_LPS_MONOCYTE_DN
N_GSE2706_UNSTIM_VS_2H_LPS_AND_R848_DC_DN
N_GSE9988_ANTI_TREM1_VS_ANTI_TREM1_AND_LPS_MONOCYTE_DN
T_GSE32164_RESTING_DIFFERENTIATED_VS_ALTERNATIVELY_ACT_M2_MACROPHAGE_UP
T_GSE24634_TEFF_VS_TCONV_DAY10_IN_CULTURE_UP
T_GSE25088_WT_VS_STAT6_KO_MACROPHAGE_DN

Table S1 (*continued*)

https://dx.doi.org/10.21037/tcr-24-327

Table S1 (*continued*)

T_GSE3982_MEMORY_CD4_TCELL_VS_TH2_DN
T_GSE3982_NKCELL_VS_TH1_DN
T_GSE3982_EFF_MEMORY_CD4_TCELL_VS_TH2_DN
T_GSE36826_WT_VS_IL1R_KO_SKIN_STAPH_AUREUS_INF_UP
T_GOLDRATH_EFF_VS_MEMORY_CD8_TCELL_UP
T_GSE3982_CENT_MEMORY_CD4_TCELL_VS_TH2_DN
T_GSE26156_DOUBLE_POSITIVE_VS_CD4_SINGLE_POSITIVE_THYMOCYTE_DN
T_GSE30962_ACUTE_VS_CHRONIC_LCMV_PRIMARY_INF_CD8_TCELL_DN
T_GSE45365_HEALTHY_VS_MCMV_INFECTION_CD11B_DC_DN
T_GSE11386_NAIVE_VS_MEMORY_BCELL_UP
T_GSE16451_CTRL_VS_WEST_EQUINE_ENC_VIRUS_IMMATURE_NEURON_CELL_LINE_DN
T_GSE13485_CTRL_VS_DAY7_YF17D_VACCINE_PBMC_DN
T_KAECH_DAY8_EFF_VS_MEMORY_CD8_TCELL_UP
T_GSE13485_DAY3_VS_DAY7_YF17D_VACCINE_PBMC_DN
T_GSE10239_NAIVE_VS_KLRG1HIGH_EFF_CD8_TCELL_DN
T_GSE45365_HEALTHY_VS_MCMV_INFECTION_CD11B_DC_IFNAR_KO_DN
T_GSE24634_IL4_VS_CTRL_TREATED_NAIVE_CD4_TCELL_DAY7_UP
T_GSE28726_NAIVE_VS_ACTIVATED_CD4_TCELL_DN
T_GSE2405_S_AUREUS_VS_UNTREATED_NEUTROPHIL_DN
T_GSE45365_WT_VS_IFNAR_KO_BCELL_MCMV_INFECTION_DN
T_GSE40274_CTRL_VS_EOS_TRANSDUCED_ACTIVATED_CD4_TCELL_UP
T_GSE13547_CTRL_VS_ANTI_IGM_STIM_BCELL_2H_UP
T_GSE13547_2H_VS_12_H_ANTI_IGM_STIM_ZFX_KO_BCELL_DN
T_GSE28726_NAIVE_CD4_TCELL_VS_NAIVE_VA24NEG_NKTCELL_UP
T_GSE39110_DAY3_VS_DAY6_POST_IMMUNIZATION_CD8_TCELL_WITH_IL2_TREATMENT_UP
T_GSE45365_WT_VS_IFNAR_KO_CD11B_DC_MCMV_INFECTION_DN
T_GSE12845_IGD_POS_BLOOD_VS_PRE_GC_TONSIL_BCELL_DN
T_GSE25088_WT_VS_STAT6_KO_MACROPHAGE_IL4_STIM_DN
T_GSE13547_2H_VS_12_H_ANTI_IGM_STIM_BCELL_UP
T_GSE39110_DAY3_VS_DAY6_POST_IMMUNIZATION_CD8_TCELL_DN
T_GSE14415_TCONV_VS_FOXP3_KO_INDUCED_TREG_DN
T_GSE14415_INDUCED_VS_NATURAL_TREG_DN
T_GSE13547_CTRL_VS_ANTI_IGM_STIM_BCELL_12H_UP
T_GSE24634_TEFF_VS_TCONV_DAY7_IN_CULTURE_UP
T_GSE14415_NATURAL_TREG_VS_TCONV_DN
T_GSE15750_DAY6_VS_DAY10_EFF_CD8_TCELL_UP

BC, bladder cancer.

https://dx.doi.org/10.21037/tcr-24-327

Table S2 The 20 representative prognosis-related gene sets in BC subtypes are identified by univariate Cox regression analysis

id	HR	HR.95L	HR.95H	pvalue
N_GSE1460_CD4_THYMOCYTE_VS_THYMIC_STROMAL_CELL_DN	1,955.7124	52.861109	72,355.861	3.90E-05
N_HALLMARK_EPITHELIAL_MESENCHYMAL_TRANSITION	10.094612	2.4250258	42.020661	0.0014862
N_GSE6259_CD4_TCELL_VS_CD8_TCELL_UP	1,240.9502	24.347049	63,250.267	0.0003829
N_GSE1460_INTRATHYMIC_T_PROGENITOR_VS_THYMIC_STROMAL_CELL_DN	388.4133	16.241028	9,289.1219	0.0002323
N_GSE26488_WT_VS_HDAC7_DELTAP_TG_OT2_THYMOCYTE_WITH_PEPTIDE_INJECTION_DN	12,414.218	82.565572	1,866,550.4	0.0002282
N_GSE4748_CTRL_VS_LPS_AND_CYANOBACTERIUM_LPSLIKE_STIM_DC_3H_UP	444.2844	8.9548426	22,042.669	0.00221
N_HALLMARK_APICAL_JUNCTION	201.6031	4.8516776	8,377.2696	0.0052625
N_GSE4748_CTRL_VS_LPS_STIM_DC_3H_UP	474.04836	13.815365	16,266.081	0.0006364
N_GSE1432_6H_VS_24H_IFNG_MICROGLIA_UP	463.08245	3.6617548	58,563.549	0.0129344
N_GSE8868_SPLEEN_VS_INTESTINE_CD11B_POS_CD11C_NEG_DC_DN	1,457.3729	6.0379319	351,765.42	0.0092597
N_GSE3982_DC_VS_BCELL_UP	125.63682	2.3850326	6,618.1946	0.0168613
N_GSE43955_1H_VS_42H_ACT_CD4_TCELL_WITH_TGFB_IL6_DN	469.4618	2.8868703	76,343.709	0.0178805
N_HALLMARK_HYPOXIA	86.822483	1.5269002	4,936.8936	0.0303676
T_GSE2706_UNSTIM_VS_2H_LPS_DC_UP	0.000419	1.54E-06	0.1142713	0.0065673
N_GSE9988_ANTI_TREM1_VS_CTRL_TREATED_MONOCYTES_UP	37.43445	1.0495922	1,335.1262	0.0469772
N_GSE36891_UNSTIM_VS_POLYIC_TLR3_STIM_PERITONEAL_MACROPHAGE_UP	24.76714	1.2664715	484.34664	0.0343714
T_GSE32164_RESTING_DIFFERENTIATED_VS_ALTERNATIVELY_ACT_M2_MACROPHAGE_UP	157.48352	2.2281883	11,130.594	0.0198728
T_GSE25088_WT_VS_STAT6_KO_MACROPHAGE_DN	52.396331	1.9097451	1,437.5612	0.0191375
T_GSE3982_MEMORY_CD4_TCELL_VS_TH2_DN	98.194238	1.241716	7,765.1478	0.0396812
T_GSE45365_HEALTHY_VS_MCMV_INFECTION_CD11B_DC_DN	29.851438	1.1207532	795.09775	0.0425563

BC, bladder cancer.

Table S3 A prognostic model containing seven gene sets was established by the LASSO analysis

Gene	Coef
N_GSE1460_CD4_THYMOCYTE_VS_THYMIC_STROMAL_CELL_DN	9.4789547
N_GSE26488_WT_VS_HDAC7_DELTAP_TG_OT2_THYMOCYTE_WITH_PEPTIDE_INJECTION_DN	4.7435145
N_HALLMARK_APICAL_JUNCTION	–0.56884
N_GSE1432_6H_VS_24H_IFNG_MICROGLIA_UP	–5.037914
N_GSE43955_1H_VS_42H_ACT_CD4_TCELL_WITH_TGFB_IL6_DN	–2.133411
N_HALLMARK_HYPOXIA	–1.829146
T_GSE25088_WT_VS_STAT6_KO_MACROPHAGE_DN	3.0210103

LASSO, least absolute shrinkage and selection operator.

https://dx.doi.org/10.21037/tcr-24-327